CORRELATION OF MICRO- AND MACROSCOPIC STRUCTURES OF WIND WAVES AND DIFFERENTIAL ROUGHENING AND SMOOTHING OF SURFACE WAVES BY WIND

Jin Wu

Hydronautics, Incorporated

Prepared for:

Office of Naval Research
Advanced Research Projects Agency

November 1973

ib

HYDRONAUTICS, Incorporated

TECHNICAL REPORT 7211-6

CORRELATION OF MICRO- AND MACROSCOPIC STRUCTURES OF WIND WAVES AND DIFFERENTIAL ROUGHENING AND SMOOTHING OF SURFACE WAVES BY WIND

By

Jin Wu

November 1973

Sponsored by

Advanced Research Projects Agency
ARPA Order No. 1910, Amendment No. 5
Under
Contract N00014-72-C-0509
NR 062-472

UNCLASSIFIED

SECURITY CLASSIFICATION OF THIS PAGE (When Data Entered)

AD 772 634

REPORT DOCUMENTATION PAGE		READ INSTRUCTIONS BEFORE COMPLETING FORM
1. REPORT NUMBER T. R. 7211-6	2. GOVT ACCESSION NO.	3. RECIPIENT'S CATALOG NUMBER
4. TITLE (and Subtitle) CORRELATION OF MICRO- AND MACROSCOPIC STRUCTURES OF WIND WAVES AND DIFFERENTIAL ROUGHENING AND SMOOTHING OF SURFACE WAVES BY WIND		5. TYPE OF REPORT & PERIOD COVERED Technical Report 6. PERFORMING ORG. REPORT NUMBER T. R. 7211-6
7. AUTHOR(s) Jin Wu		8. CONTRACT OR GRANT NUMBER(s) N00014-72-C-0509
9. PERFORMING ORGANIZATION NAME AND ADDRESS HYDRONAUTICS, Incorporated 7210 Pindell School Rd, Howard County, Laurel, Md. 20810		10. PROGRAM ELEMENT, PROJECT, TASK AREA & WORK UNIT NUMBERS NR 062-472
11. CONTROLLING OFFICE NAME AND ADDRESS Advanced Research Projects Agency Arlington, Va. 22209		12. REPORT DATE November 1973 13. NUMBER OF PAGES 36
14. MONITORING AGENCY NAME & ADDRESS (if different from Controlling Office) Office of Naval Research Department of Defense Arlington, Va. 22209		15. SECURITY CLASS. (of this report) UNCLASSIFIED 15a. DECLASSIFICATION/DOWNGRADING SCHEDULE

16. DISTRIBUTION STATEMENT (of this Report)

This document has been approved for public release and sale; its distribution is unlimited.

17. DISTRIBUTION STATEMENT (of the abstract entered in Block 20, if different from Report)

18. SUPPLEMENTARY NOTES

19. KEY WORDS (Continue on reverse side if necessary and identify by block number)

Wind Waves
Microstructure of Sea Surface
Roughness of Sea Surface
Wind-Wave Interaction
Wave-Wave Interaction

20. ABSTRACT (Continue on reverse side if necessary and identify by block number)

Simultaneous measurements were conducted in a wind-wave tank of the ripple slopes with an optical instrument and of the carrier-wave profiles with a wave-height gage. The experiments were conducted under various wind conditions: either steady or unsteady wind blowing over pre-existing regular surface waves. The data were analyzed to determine the slope distributions of ripples

DD FORM 1 JAN 73 1473 EDITION OF 1 NOV 65 IS OBSOLETE
S/N 0102-014-6601

UNCLASSIFIED
SECURITY CLASSIFICATION OF THIS PAGE (When Data Entered)

20. (Continued)

located on various portions of the carrier-wave profiles under steady wind, and the differential roughening and smoothing of the carrier waves under unsteady wind. The influences of pre-existing waves on the structure of the wind boundary layer, and on the slope statistics of ripples were also studied.

TABLE OF CONTENTS

LIST OF FIGURES

ABSTRACT

Simultaneous measurements were conducted in a wind-wave tank of the ripple slopes with an optical instrument and of the carrier-wave profiles with a wave-height gage. The experiments were conducted under various wind conditions: either steady or unsteady wind blowing over pre-existing regular surface waves. The data were analyzed to determine the slope distributions of ripples located on various portions of the carrier-wave profiles under steady wind, and the differential roughening and smoothing of the carrier waves under unsteady wind. The influences of pre-existing waves on the structure of the wind boundary layer, and on the slope statistics of ripples were also studied.

1. INTRODUCTION

The wind-disturbed water surface features ripples riding on long waves. There has been a great deal of interest in determining the statistical description of the microstructure of the disturbed surface, the pattern of ripples. These wavelets were considered (Phillips 1966) to be involved in the inception of wind waves as well as in the dissipation of wave energy. In addition, the microstructure was also suggested to govern the reflection and the backscattering of the electromagnetic waves (Newton and Rouse 1972) impinging on, and the radiation of thermal energy (McGrath and Osborne 1973) from, the air-sea interface.

Some measurements (Schooley 1954, Cox and Munk 1956, Cox 1958, Wu 1971a, 1972a) have been conducted in the past to determine the slope and curvature distributions of wind waves under various wind velocities. There is, however, a lack of detailed studies of the distributions of ripples along the profiles of the carrier waves and the correlations of these distributions with wind and wave conditions. Such distributions are helpful for understanding energy transfer processes from wind to waves (Longuet-Higgins 1969, Wu 1972b), and between wave components (Longuet-Higgins 1963, Phillips 1963). These distributions are also helpful for setting the viewing angle of the microwave sensor over the sea surface and interpreting results of microwave measurements. It should also be pointed out that all the past measurements of ripples were conducted under steady winds. Yet the roughening of the water surface by a suddenly started wind, and the dissipation of ripple energy following a suddenly stopped wind, should be more revealing of the mechanism of dynamic interaction between wind and waves, or even among wave components. This kind of measurement of the microstructure under unsteady wind is also desirable for modeling the air-sea interface, because the natural wind is generally unsteady.

In the present study, the carrier-wave profiles and the ripple slopes were simultaneously measured at a fixed point in a laboratory wind-wave tank under various wind velocities. For the convenience of experiments conducted under a short fetch, pre-existing regular surface waves were generated. Each series of

experiments included three phases with the following sequence of wind and wave conditions; a suddenly started wind over a calm water surface, a steady wind over an equilibrium disturbed water surface, and a suddenly stopped wind over an initially disturbed surface. Features of the correlations between the micro-and macroscopic structures of the disturbed water surface under steady winds, and patterns of the differential roughening and decay of the microstructure under unsteady winds, are herein presented.

2. EXPERIMENTAL CONDITIONS AND PROCEDURES

2.1 Equipment

The experiments have been conducted in a wind-wave tank, which is 1.5 m wide and 22 m long. Mounted at the upwind end of the tank is an axial-flow fan, driven by a variable-speed motor; a permeable wave absorber is installed at the downwind end. The tank is covered for the first 15 m to provide a 0.31-m high wind tunnel above 1.24-m deep water. The maximum obtainable wind velocity within the tunnel is 14 m/s. The test section is located at the middle length of the tank.

The tank is also equipped with a mechanical wave generator, a flap with its lower edge hinged at the bottom of the tank and with its upper edge oscillated at any desired frequency and amplitude by a motor. The fan and the mechanical wave generator can be operated either separately or simultaneously.

2.) Wind and Wind Measurements

The differential roughening and smoothing of the regular waves were studied with a suddenly started and a suddenly stopped wind, respectively. The instantaneous starting or stopping of the wind was achieved by means of a curtain supported at the air intake of the fan. The curtain can be either rolled up around a metal pipe attached at its lower edge, or hung in front of the intake. When the fan turns, the curtain is sucked against the heavy-wire grid at the intake to block completely the airflow. For measurements of wave decay, the curtain is up initially while the wind blows steadily to build up an equilibrium microstructure in the tank. Subsequently, the fan is turned off and at the same time the metal pipe is released to drop the curtain. For measurements of wave growth, the curtain is down while the fan is turned on to build up the required speed. Subsequently, the curtain is suddenly rolled up around the metal pipe. It was determined that one second was required to cover completely the fan section and one and one-half seconds was necessary to open it up completely. Such an arrangement with the curtain is needed, because the mechanical inertia of the fan makes it impossible to either start or stop the airflow suddenly. Following the lift or drop of the curtain, the energy supplied by the wind was either suddenly present or completely cut off, and the microstructure in the tank varied rapidly.

The velocity distributions of steady winds blowing over pre-existing waves were determined with a pitot-static probe and a differential pressure transducer unit. The probe was supported

successively at various elevations above the water surface. The output of the pressure transducer, which is proportional to the square of the velocity, was first fed to a square-root circuitry and then displayed on an x-y plotter. At each elevation, the velocity was continuously recorded for a period of 30 seconds. The latter is much longer than the period of surface waves, and the average wind velocity at each elevation can be determined.

2.3 Waves and Wave Measurements

Two types of instruments have been used simultaneously in this experiment: a conductivity probe for recording carrier-wave profiles and an optical instrument for measuring ripple slopes. The conductivity probe consists primarily of a partially submerged platinum wire, supported vertically at the test section. The output of the electric current flowing through the probe is proportional to the submergence of the wire. The probe, however, does not provide enough resolution for measuring wavelets that ride on top of long waves and have amplitudes only a fraction of the latter.

The optical instrument consists principally of a light source and a telescope and photomultiplier unit. Supported over the wind-wave tank, the instrument can be set at any desired inclination from the water surface. The photomultiplier receives reflected light only when the water surface is normal to the plane containing the light sheet and the telescopic axis. The cross sections of the light sheet is rectangular with a large length-to-width

ratio and with its short side aligned with the direction of the wind. The instrument is, therefore, insensitive to the crosswind slope; the angular tolerance of the instrument to the water surface slope is about 1° in the longitudinal (wind) direction and is about 20° in the transverse direction. During the experiment, the instrument was set successively at various inclinations to measure the frequencies of occurrence of the corresponding upwind-downwind slopes of the disturbed surface. A detailed description of the instrument has been reported earlier (Wu 1971a).

For the major portion of the measurements, the outputs of the wave-height gage and of the optical instrument were recorded simultaneously on different channels of a tape recorder. Details of these measurements and data processing — correlation between micro-and macroscopic structures, growth and decay of ripples over carrier waves — will be discussed in later sections.

Since the wind-induced drift is known (Phillips 1973a, Wu 1973a) to modify the propagation of surface waves, additional experiments were conducted to measure the carrier waves under various wind velocities. As the wind blew harder, the carrier waves became more and more sharply peaked, but remained regular. Two wave probes were used during this part of the experiment: the upwind probe was fixed and the downwind probe was supported on a sliding scale. The distance between probes was adjusted to make the wave signals from two probes, monitored on the scope, oscillating in phase. This distance is therefore the wavelength. The heights and lengths of carrier waves under various wind velocities are shown in Figure 1. On the other hand, the wave

height is seen to increase slowly at low wind velocities, more effectively at medium wind velocities, and again slowly at high wind velocities where violent wave breaking occurs. The variation of the wavelength with the wind velocity appears to be consistent with that of the wave height; where the wave height increases more effectively with the wind velocity, the wavelength increases less effectively.

2.4 Correlation Measurements

The signals of the photomultiplier produced by the wind-disturbed water surface are light pulses having various intensities and various durations. The intensity is related to the surface curvature (Wu 1972a) and the duration is the period for transferring under the instrument a slope within the slope-tolerance limit (1^{o}) of the optical instrument. The period and the intensity of the pulse were not measured here, and each signal was reshaped as a pulse of a constant duration and intensity. Each shaped pulse, therefore, represents the occurrence of a given slope of the water surface regardless of its transferring speed and its curvature.

For the correlation measurements under steady wind, the carrier-wave profile was divided into four regions: upper and lower halves of either the windward or the leeward face. A gating device was designed for partitioning and collecting the light signals from each region. During the operation, the tape was played back at one quarter of the recording speed with the carrier-wave profile monitored on the oscilloscope and with the pulse signal passing through the gating device. The latter was controlled

by an operator who watched the slow varying carrier waves shown on the scope. The gating device was operated so as to feed only the light pulses from the desirable portion of the carrier-wave profile to the pulse analyzer. The tape was repeatedly run to obtain successively the data for the following portions of the carrier-wave profile: (1) the leeward face, (2) the upper half of the leeward face, and (3) the upper half of the windward face. On the basis of these three sets of data, in addition to the data obtained from the entire carrier-wave profile, the results for all four regions mentioned earlier can be deduced.

2.5 Growth and Decay Measurements

When the tape was played back, the number of pulses was also accumulated on a counter. Under a steady wind, the accumulation of the equilibrium-state data could be started at an arbitrary point of the tape. For the wave growth and decay data, the accumulation was started immediately following the identification signal indicating the instant when the wind was either suddenly started or completely stopped. The number of pulses accumulated on the counter was sampled by a printer. The sampling rate can be varied, with the maximum rate at eight numbers per second. The printout is, therefore, the temporal accumulation of the frequency of occurrence of a given water-surface slope following the change of wind conditions. For each wind velocity this process was repeated for various water-surface slopes.

3. WIND BOUNDARY LAYER OVER PRE-EXISTING WAVES

3.1 Wind-Velocity Profiles

The wind velocity profiles in the tunnel over the pre-existing regular waves are plotted in Figure 2a, b, where u is the wind velocity measured at the distance y above the mean water surface. Two series of velocity surveys were performed with pre-existing regular waves of the same frequency but different amplitudes. Series (a) with larger wave amplitudes is the primary series under which the experiments on correlation, and differential roughening and smoothing were conducted; series (b) is the secondary series, which was performed only to study effects of pre-existing waves on the wind boundary layer.

The wind velocity is seen in Figure 2 to follow the logarithmic law (Schlichting 1968, Chapter XIX), or to vary linearly with the logarithm of the distance above the water surface. The wave-induced air motion, however, is considerable near the water surface where the data are greatly scattered. This portion of the data, generally having a smaller gradient, is omitted from Figure 2. The distorted region appears to extend further away from the water surface for waves of larger amplitudes. This is not only illustrated by the data obtained under various wind velocities shown separately in Figure a, b, but also from the comparison of the logarithmic profile shown in Figure 2b with that for the corresponding wind velocity shown in Figure 2a.

3.2 Effects of Pre-Existing Waves on Wind Boundary Layer

The shear velocity (u_*) of the wind and the roughness length (k) of the disturbed water surface, calculated from the velocity profile shown in Figure 2, are plotted in Figure 3a, b. The wind velocity U shown in Figure 3 is that measured at 2/3 of the tunnel height above the mean water surface. The solid lines shown in the figure indicate the results obtained at the same test section with wind blowing over initially calm water surface (Wu 1973b). The effects of pre-existing waves on wind boundary layer are better illustrated through the results of the roughness length than those of the shear velocity; see Figure 3a, b. The roughness length, which is related to the intercept of the wind profile, is more sensitive to a small change of the velocity gradient than the shear velocity, which are related to the slope of the profile.

Similar to earlier results with wind blowing over initially calm water surface, the data of shear velocity and roughness length obtained here with pre-existing waves are divided into two groups according to whether wind-wave interaction is governed by surface tension or gravity. The shear velocity increases gradually with the wind velocity in the former regime, and rapidly in the latter regime. The roughness length decreases with the wind velocity in the former regime, and increases with the wind velocity in the latter regime. Physically, these two regimes correspond respectively, to the presence of parasitic capillaries, and to the occurrence of airflow separation and wave breaking. Without pre-existing waves, the dividing velocity of these two regimes is

about 9 m/s. With pre-existing waves, this velocity is lowered to 7 m/s, at which wave breaking starts. In other words, the pre-existing waves concentrate the energy transfer from wind to waves of a particular length and therefore promote wave breaking at its crest.

At low wind velocities in the surface-tension governing regime of wind-wave interaction, the pre-existing waves are seen in Figure 3b to smooth the water surface hydrodynamically. With pre-existing waves, the carrier waves of parasitic capillaries are much longer. Consequently, the number of capillaries per unit area of the water surface is greatly reduced. Therefore, inasmuch as the capillaries govern the dissipation of wave energy, the water surface becomes smoother with long pre-existing waves. The surface with large-amplitude, pre-existing waves is seen in Figure 3b to be hydrodynamically smoother than that with small-amplitude pre-existing waves. Because the regularity of carrier waves in the latter case was somewhat disrupted by the wind, short gravity waves with parasitic capillaries were observed superimposing on long carrier waves.

At high wind velocities in the gravity governing regime of wind-wave interaction, the airflow separation from wind waves occurs in the present tank (Wu 1968). In this case, with the wind blowing over initially calm water, the roughness length was found to be comparable to the wave height. The separation pocket is likely to cover a major portion of the windward face of the next wave. With pre-existing waves, the peak of carrier waves is again

sharply cusped, and the airflow separation from the peak should again occur. However, the separation pocket near the cusped peak, although larger in volume than that taking place without pre-existing waves, can hardly reach the windward face of the next wave. In other words, with pre-existing waves, the separation pockets are likely to be further isolated, and the density of roughness element is therefore reduced. Since the aerodynamic roughness depends on both the height and the density of the roughness elements (Schlichting 1968, Chapter XX), the more widely spaced separation pockets due to pre-existing waves cause a reduction of the roughness length. Consequently, the roughness length with pre-existing waves is smaller than the wave height. Very little difference of the roughness length is seen in Figure 3b between two cases with pre-existing waves of the same frequency (length) but different amplitudes, because for these two cases the roughness length is probably governed more by the spacing than by the height of the roughness elements.

4. CORRELATION OF MICRO- AND MACROSCOPIC STRUCTURES OF WIND WAVES

The present experiment was conducted with wind waves superimposed on pre-existing regular surface waves. The use of mechanically generated waves is necessary not only for the study of differential roughening and smoothing to be discussed in the next section, but also for the correlation study. Otherwise it would be very tedious to apply the gating technique to high-frequency, irregular carrier waves. With wind blowing over pre-existing

low-frequency waves, on the other hand, the carrier waves remain regular and the undulation of the water surface can be more easily traced by the operator. In other words, the pre-existing waves also serve as the regulator for the present correlation measurements.

4.1 Slope Distributions

The data obtained directly from the tape include the slope distributions of ripples riding on the tops of the following portions of the carrier-wave profile: (a) entire profile, (b) leeward face, (c) upper half of leeward face, and (d) upper half of windward face. From these data, the slope distribution for ripples riding on the top of the other portions of the carrier-wave profiles can be deduced: (a) windward face, (b) lower half of windward face, and (c) lower half of leeward face. The results for four different wind velocities are shown in Figure 4, one column for each wind velocity. Each row in Figure 4 indicates the data obtained from the same portion of the carrier-wave profile. The positive angle shown in the figure corresponds to a leeward slope, and the negative angle corresponds to a windward slope. The data shown in Figure 4 were obtained from a one-minute run of the experiment. A smooth curve was fitted by eye to each set of data to indicate a faired slope distribution.

The maximum frequency of occurrence of water-surface slope should be produced by the peak and the trough of ripples. Since they are tilted by the carrier waves, the peaks and troughs of ripples do not have zero slopes. Consequently, the slope distribution for ripples riding on the leeward face of carrier waves

is peaked at a positive angle, and that for ripples riding on the windward face is peaked at a negative angle. This trend is clearly illustrated by the results shown in Figure 4. At low wind velocities (U = 4.18, 6.92 m/s), the peakedness of the slope distribution for the leeward face is much stronger than that for windward face due to the presence of parasitic capillaries on the leeward face. Such a difference disappears at high wind velocities, where ripples distributed more venly over the leeward and the windward faces of carrier waves.

4.2 Effects of Pre-Existing Waves on Mean-Square Surface Slope

The mean-square slopes of the disturbed water surface with pre-existing waves were determined from the slope distributions shown on the top row of Figure 4. The results are tabulated in Table 1.

TABLE 1

Mean-Square Slopes Measured with and without Pre-Existing Waves

Wind Velocity, U (m/s)			4.18	6.92	9.60	12.25
Shear Velocity, u_* (m/s)			0.223	0.298	0.683	1.05
Mean-Square Surface Slope	With	Pre-existing Waves	0.0179	0.0219	0.0434	0.0527
	Without		0.0248	0.0426	0.0734	0.0921

The shear velocity shown in Table 1 is the faired value obtained from Figure 3a. The mean-square slopes of the disturbed water surface without pre-existing waves were measured earlier (Wu 1972a, 1973c), and were related to the shear velocity of the wind. The bottom row of Table 1 was obtained from earlier results.

For the same wind-shear velocity, mean-square slope with pre-existing waves is seen in Table 1 to be smaller than that without. This is in line with the earlier discussion concerning the roughness length. With long pre-existing waves, the patches of parasitic capillaries and the zones of wave breaking are more widely spaced. Consequently, the density of roughness elements, or number of ripples per unit area of the water surface, is reduced. In addition, there appears to be a spectral gap with ripples superimposing long carrier waves, as waves of intermediate lengths are missing. The mean-square slope of the water surface is therefore reduced, since the roughness elements and short carrier waves are the major contributor of the mean-square slope.

Even compared on the basis of wind-shear velocities, the upwind-downwind component of the mean-square water-surface slopes measured in laboratory tanks were shown (Wu 1971a) to be smaller than the oceanic results. This discrepancy was considered earlier to be due in part, to the narrowness of the tank limiting the development of the crosswind component of the mean-square slope. The present results apparently suggest another contributing factor

of this still not fully explained discrepancy. The long carrier waves in the open ocean may cause the reduction of mean-square slopes.

4.3 Distribution of Ripples along Carrier-Wave Profiles

As discussed in the previous section, the maximum frequency of occurrence of the water-surface slope, or the peak of the slope-distribution curve, appears to correspond to twice the number of ripples. Composite pictures showing the distributions of ripples on various segments of carrier-wave profiles at different wind velocities are presented in Figure 5. The four numbers indicated along the wave profile are the relative frequencies of occurrence of ripples riding on four respective segments of the carrier-wave profile, the numbers on top of the profile are the relative frequencies for the windward and the leeward faces, and the numbers on the right side are those for the upper and the lower half of the profile. At high wind velocities (U = 9.60, 12.[illegible] m/s) the carrier-wave profile becomes skewed with shorter leeward face and longer windward face. The numbers in parentheses are the weighted values taking the skewness of the carrier-wave profile into consideration.

On the basis of these composite pictures, the distribution of surface roughnesses appear to have the following features:

(a) At low wind velocities (U = 4.18, 6.92 m/s) of the surface-tension governing regime of wind-wave interaction, the leeward face of the carrier wave is much rougher than the windward face due to the presence of parasitic capillaries.

(b) At high wind velocities (U = 9.60, 12.25 m/s) of gravity-governing regime of wind-wave interaction, the general trend is that as the wind velocity increases the overall difference on roughening between leeward and the windward faces becomes less.

(c) In the surface-tension governing regime of wind-wave interaction at two low wind velocities, the parasitic capillaries are concentrated near the upper half of the leeward face at U = 4.18 m/s, and move further down the leeward face at U = 6.92 m/s.

(d) The breaking of wind waves (without pre-existing mechanically generated surface waves) was observed earlier (Wu 1971b) to occur on the leeward face but very close to the wave peak. Excessive roughness should therefore be concentrated on the upper half of the leeward face of the carrier-wave profile. With pre-existing waves, however, the relative frequency of occurrence of ripples on the upper half of the windward face at U = 9.60 and 12.25 m/s is seen in Figure 5 to be greater than that on the windward face. This is somewhat surprising observations. It is worth noting that the bubbling of the water surface and the three-dimensional type roughness accompanying wave breaking may escape the optical counting technique, but not the glitter photography (Wu 1971t).

(e) The lower half of the windward face is the smoothest segment of the carrier-wave profile.

5. DIFFERENTIAL ROUGHENING AND SMOOTHING OF A WAVY SURFACE

For a steady wind, the frequency of occurrence of a given water-surface slope (that is, the rate of light pulses detected by the optical instrument at a given angle of inclination) for an equilibrium, random wind-disturbed water surface should be nearly constant, $\bar{r}$. The equilibrium-state data were discussed in the previous section, and the distributions of $\bar{r}$ obtained from various segments of the carrier-wave profiles and under different wind velocities are presented in Figure 4.

In order to study the differential roughening of a wavy surface by wind and the differential decay of wind-excited ripples on a wavy surface, suddenly started and suddenly stopped winds were introduced. The frequencies of occurrence of water-surface slopes were determined with the optical instrument both during the growth stage (r_g) following a suddenly started wind, and during the decay stage (r_d) following a suddenly stopped wind. Applying the same procedure as that used earlier for the steady-state data, the growth and decay data were first obtained from certain portions of the carrier-wave profile, and subsequently, the results for the other portions of the profile were deduced. The data for the growth stage were obtained from a period of one minute, and those for the decay stage were obtained from a period

of 30 seconds. The sampling interval of the printer is one second for the growth stage and is one-half of one second for the decay stage.

5.1 Growth and Decay of Root-Mean-Square Slopes

The values r_g and r_d are the frequencies of occurrence of a particular water-surface slope at a given instant following, respectively, the sudden starting and the sudden stopping of the wind. At any given instant, the distribution of the water-surface slopes can be obtained by compiling the instantaneous frequencies of occurrence of various slopes. The temporal variations of the slope-distribution curves for the growth and the decay stages, not shown here, follow a general pattern; namely, widening with time for the growth stage and peaking with time for the decay stage. Details of data analysis and of temporal slope distributions are similar to those reported earlier (Wu 1973c) with wind blowing over initially calm water.

The variances of the water-surface slopes for ripples riding on various portions of the carrier-wave profiles at various times during the growth and the decay stages were calculated from the instantaneous slope distributions. Subsequently, the variances were normalized with respect to the value obtained from the entire profile of carrier waves under steady wind. The temporal variations of the normalized variances following the sudden start and the sudden stop of the wind are plotted as light lines in Figures 6 and 7, respectively. The horizontal axis in both figures indicates the time t after either the sudden start or the

sudden stop of the wind. Generally, the data illustrates an exponential growth and an exponential decay of the water-surface slopes with time.

Two exponential curves of the following forms were fitted on the basis of the least-squares principles to the wave growth and decay data, respectively:

$$(\overline{s_g^2})^{\frac{1}{2}} \Big/ (\overline{s_o^2})^{\frac{1}{2}} = \exp(-t/T_g)$$

and [1]

$$(\overline{s_d^2})^{\frac{1}{2}} \Big/ (\overline{s_o^2})^{\frac{1}{2}} = \exp(-t/T_d)$$

$(\overline{s_g^2})^{\frac{1}{2}}$ and $(\overline{s_d^2})^{\frac{1}{2}}$ are the root-mean-square slopes at time t during, respectively, the growth and the decay stage; $(\overline{s_o^2})^{\frac{1}{2}}$ is the steady state root-mean-square slope; T_g and T_d are the respective relaxation times for the growth and the decay of the mean-square slope. The fitted exponential curves are shown as the heavy lines in Figures 6 and 7. The data are seen in both figures to follow reasonably closely the fitted curves. The scatter of the data can not be avoided here, as the interval between data points is only one second.

5.2 Effects of Pre-Existing Waves on Growth and Decay of Ripples

The relaxation times for the growth and the decay of ripples over long pre-existing waves were obtained from Figures 6 and 7, and are tabulated in Table 2. The same times scales without pre-existing waves were reported earlier (Wu 1973c), and their values for the corresponding wind-shear velocities are also shown in Table 2.

TABLE 2

Relaxation Time Scales of Growth and Decay of Ripples With and Without Pre-Existing Waves

Wind Velocity U (m/s)	Growth Time, T_g (sec)		Decay Time, T_d (sec)	
	With	Without	With	Without
	Pre-Existing Waves			
4.18	2.13	7.7	93.4	28
6.92	2.32	4.2	69.0	25
9.60	3.13	0.9	44.6	17
12.25	4.17	0.1	50.3	18

A time lag between the sudden start of the wind and the exponential growth of root-mean-square surface slopes was observed earlier (Wu 1973c) in the present tank without pre-existing waves. Such a time lag is not seen in Figure 6. The growth time T_g shown in Table 2 for the case without pre-existing waves is that obtained from the earlier study with the time for wind initiation delayed by the time lag.

The growth times with pre-existing waves are seen in Table 2 to be shorter than those without at low wind velocities, and longer than those without at high wind velocities. Inasmuch as the shear velocities are the same for both cases, the difference is therefore merely due to the change of surface wave structures. The shortened growth time in the surface-tension governing regime with

parasitic capillaries may be due to the fact that a certain time is required for the carrier waves to develop from an initially calm water surface while the carrier waves already exist in the present experiment. The lengthened growth time in the gravity governing regime may be explained in the similar fashion as in the previous section regarding the effects of pre-existing waves on the mean-square slopes. The results at high wind velocities may be applicable to the oceanic condition, while the condition for the low wind velocities may exist only in laboratory wind-wave tanks (Wu 1970).

The decay times with pre-existing waves are seen in Table 2 to be much longer than those without for all wind velocities. This is apparently due to the slow damping of long carrier waves, and very active wave-wave interaction with ripples deriving energy from long carrier waves.

5.3 Differential Roughening and Smoothing of Wavy Surfaces

The growth and decay times for various segments of the carrier-wave profiles were obtained as discussed previously and are tabulated in Table 3. The general trends of the results are:

(1) There is no systematic indication of differential roughening of the windward and the leeward faces in either surface tension or gravity governing regime of wind-wave interaction.

(2) At the lowest wind velocity, the growth time is the longest for the upper half of leeward face, where parasitic capillaries are concentrated.

At the highest wind velocity, the growth is again the longest for the same segment of the wave profile, where violent wave breaking takes place. These trends are also true for the other wind velocities.

TABLE 3

Relaxation Times for Ripples Riding on Various Portions of Carrier-Wave Profiles

Relaxation Time (sec)		Growth Time, T_g				Decay Time, T_d			
Wind Velocity, U(m/s)		4.18	6.92	9.60	12.25	4.18	6.92	9.60	12.25
Portion of Carrier Wave Profile	Entire Profile	2.13	2.32	3.13	4.17	93.4	69.0	44.6	50.5
	Leeward Face	3.14	2.09	3.09	4.19	94.5	74.4	42.2	41.5
	Windward Face	1.33	3.21	3.24	4.12	57.4	57.5	47.4	58.6
	Upper Half Leeward Face	4.02	2.12	3.31	7.34	125.5	48.7	32.6	19.5
	Lower Half Leeward Face	1.12	1.18	1.12	2.22	82.7	86.5	48.6	97.5
	Upper Half Windward Face	2.22	4.15	3.42	3.14	53.3	56.5	47.0	22.7
	Lower Half Windward Face	1.92	2.62	2.12	4.52	87.0	88.0	96.0	62.7

(3) The lower half of the leeward face is seen to provide the fastest response of the wind excitation.

(4) Opposite trends are seen at low and high wind velocities for the differential smoothing of the leeward and the windward faces. However, it is not clear why this is the case.

(5) The lower half of the windward face appears to have the fastest decay of ripple energy.

6. CONCLUDING REMARKS

The results obtained from the present experimental studies are summarized below:

(1) Effects of Pre-Existing Waves on Wind Boundary Layer and Microstructure: The effects of long pre-existing waves on the structures of wind and ripples are consistent. Compared on the basis of the wind-shear velocity, the roughness length of the wind boundary layer and the mean-square slope of the water surface are smaller with pre-existing waves than without. The reduction of mean-square slope by long carrier waves appear to provide a probable explanation of why the laboratory determined values are larger than oceanic ones, again compared on the basis of the wind-shear velocity.

(2) Correlation of Micro- and Macrostructures: The slope distributions of ripples on various segments of the carrier-wave profiles are skewed. In the surface-tension governing regime of wind-wave interaction, the leeward face is much rougher than the windward face. The parasitic capillaries are concentrated on the upper half of the leeward face at a lower wind velocity, and move further downward

at higher wind velocities. In the gravity governing regime, the difference in roughness between the leeward and the windward faces becomes smaller. However, the roughness on the windward face is concentrated on the upper half of the wave profile; the lower half of the windward face is the smoothest segment of the long wave profile. These observations may be helpful for setting the viewing angle of the microwave sensors, and for interpreting the results of the microwave measurements.

(3) Differential Roughening and Smoothing of Long Surface Waves: Small differences in roughening and smoothing of various segments of the carrier-wave profile were found. An important finding in this part of the study is that pre-existing waves affect the growth and the decay time scales of mean-square surface slopes, especially those at high wind velocities. The wind and wave conditions at high wind velocities are similar to oceanic conditions. The relaxation time scales are found to be much longer with than without the presence of long carrier waves. The presence of long waves eliminates wave components of intermediate lengths and extracts the energy introduced by the wind through ripples. These results are believed to be important for studying wind-wave-current interactions.

REFERENCES

Cox, C. S. and Munk, W. H., 1956, "Slopes of the Sea Surface Deduced from Photographs of Sun Glitter," 6, No. 9, Scripps Institution of Oceanography.

Cox, C. S., 1958, "Measurements of Slopes of High-Frequency Wind Waves," J. Mar. Res. 16, 199-225.

Longuet-Higgins, M. S., 1963, "The Generation of Capillary Waves by Steep Gravity Waves," J. Fluid Mech. 16, 138-59.

Longuet-Higgins, M. S., 1969, "A Nonlinear Mechanism for the Generation of Sea Waves," Proc. Roy. Soc. A311, 371-89.

McGrath, J. R. and Osborne, M.F.M., 1973, "Some Problems Associated with Wind Drag and Infrared Images at Sea Surface," J. Phys. Oceangr. 3, 318-27.

Newton, R. W. and Rouse, J. W., Jr., 1972, "Experimental Measurements of 2.25-cm Backscatter from Sea Surfaces," IEEE Trans. GE-10, 2-7.

Phillips, O. M., 1963, "On the Attenuation of Long Gravity Waves by Short Breaking Waves," J. Fluid Mech. 16, 321-32.

Phillips, O. M., 1966, "The Dynamics of the Upper Ocean," Cambridge University Press.

Phillips, O. M., 1973a, "The Influences of Wind Drift and Capillarity on Blockage," HYDRONAUTICS, Incorporated Technical Report 7211-1.

Phillips, O. M., 1973b, "The Regeneration of Surface Waves by Wind in Interactions with Internal Gravity Waves (U)," HYDRONAUTICS, Incorporated Technical Report 7211-2, (CONFIDENTIAL).

Schlichting, H., 1968, "Boundary-Layer Theory," 6th Ed. McGraw-Hill Book Company, New York.

Schooley, A. H., 1954, "A Simple Optical Method for Measuring the Statistical Distribution of Water Surface Slopes," J Opt. Soc. Am., 44, 37-40.

Wu, Jin, 1968, "Laboratory Studies of Wind-Wave Interactions," J. Fluid Mech. 34, 91-112.

Wu, Jin, 1970, "Wind-Wave Interactions," Phys. Fluids 13, 1926-1930.

Wu, Jin, 1971a, "Slope and Curvature Distributions of Wind-Disturbed Water Surface," J. Opt. Soc. Am. 61, 852-58.

Wu, Jin, 1971b. "Observations on Long Waves Sweeping Through Short Waves," Tellus 23, 364-70.

Wu, Jin, 1972a, "Surface Curvature of Wind Waves Observed from Different Angles," J. Opt. Soc. Am. 62, 395-400.

Wu, Jin, 1972b, "Physical and Dynamical Scales for Generation of Wind Waves," J. Waterways, Harbor Coastal Engr. Div. ASCE 98, WW2, 163-175.

Wu, Jin, 1973a, "Effects of Wind-Induced Drift Currents on the Propagation of Surface Waves," HYDRONAUTICS, Incorporated Technical Report 7211-3.

Wu, Jin, 1973b, "Wind-Induced Drift Current," HYDRONAUTICS, Incorporated Technical Report 7303-3.

Wu, Jin, 1973c, "Rates of Growth and Decay of Wind Waves under Conditions of Unsteady Wind," HYDRONAUTICS, Incorporated Technical Report 7211-4.

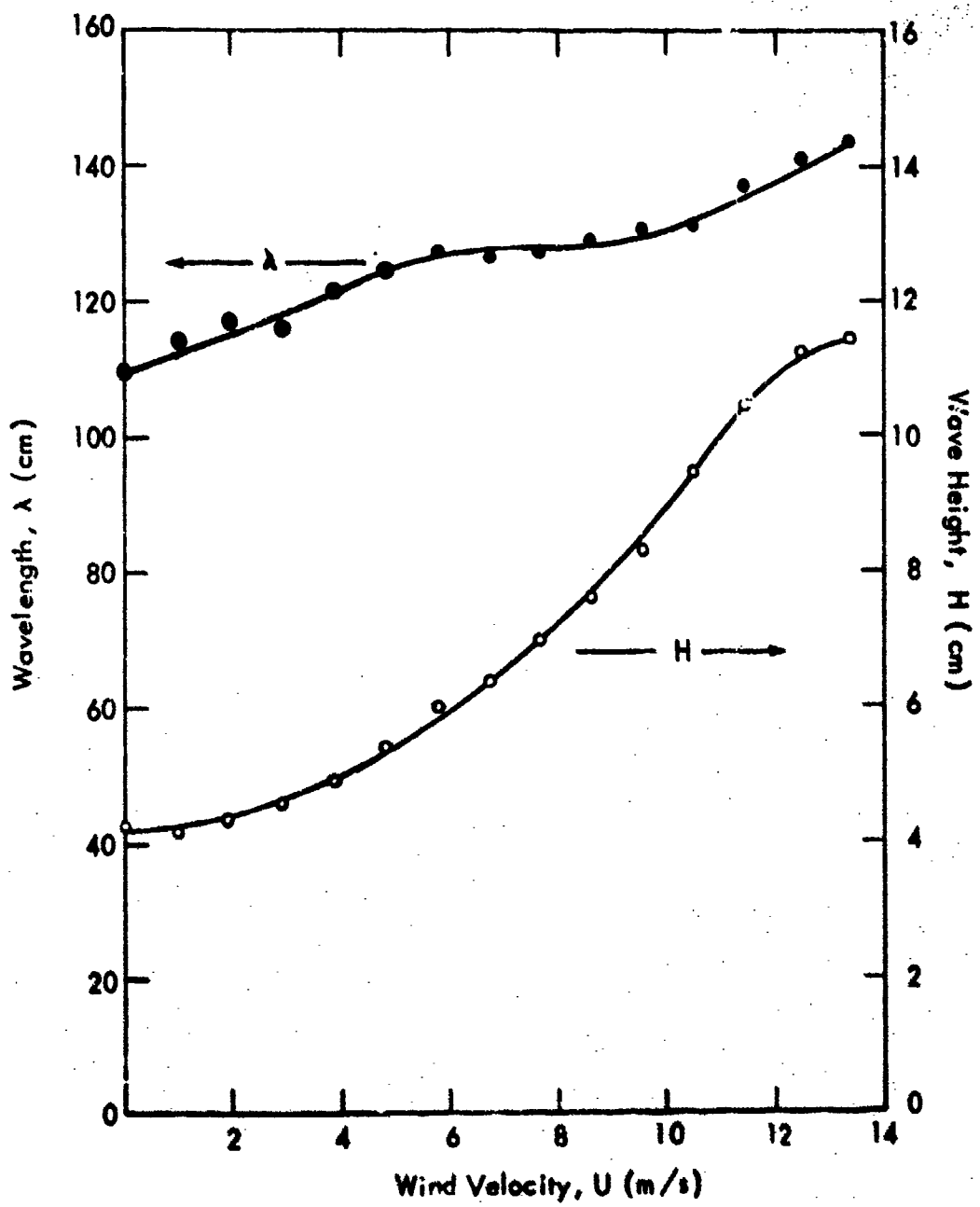

FIGURE 1 - AVERAGE WAVELENGTHS AND WAVE HEIGHTS UNDER VARIOUS WIND VELOCITIES

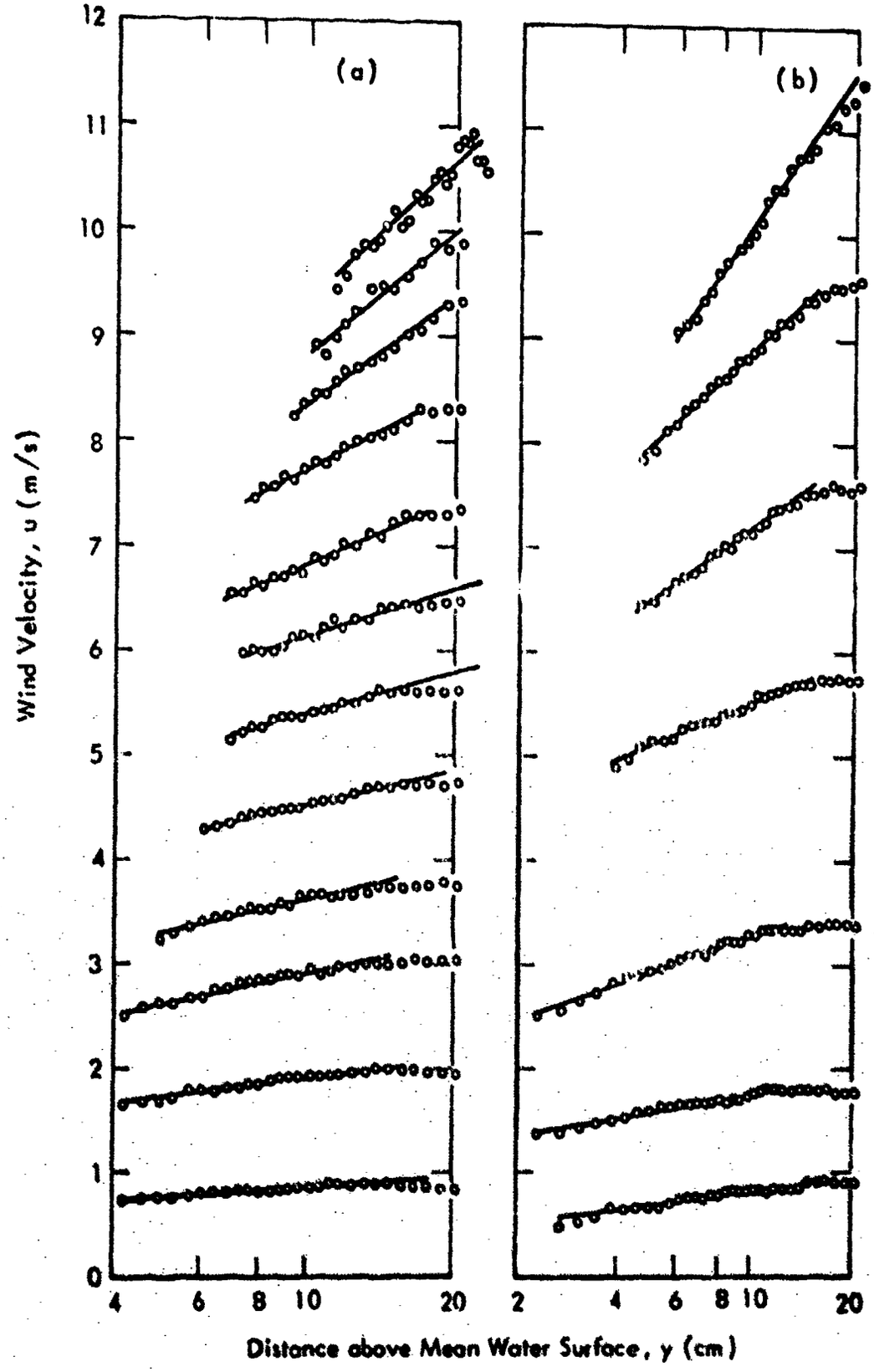

FIGURE 2 - VELOCITY DISTRIBUTIONS OF WIND BLOWING OVER PRE-EXISTING WAVES OF LARGE AMPLITUDE (a) AND OF SMALL AMPLITUDE (b). In each block the profiles were obtained from bottom to top at the order of increasing freestream wind velocities.

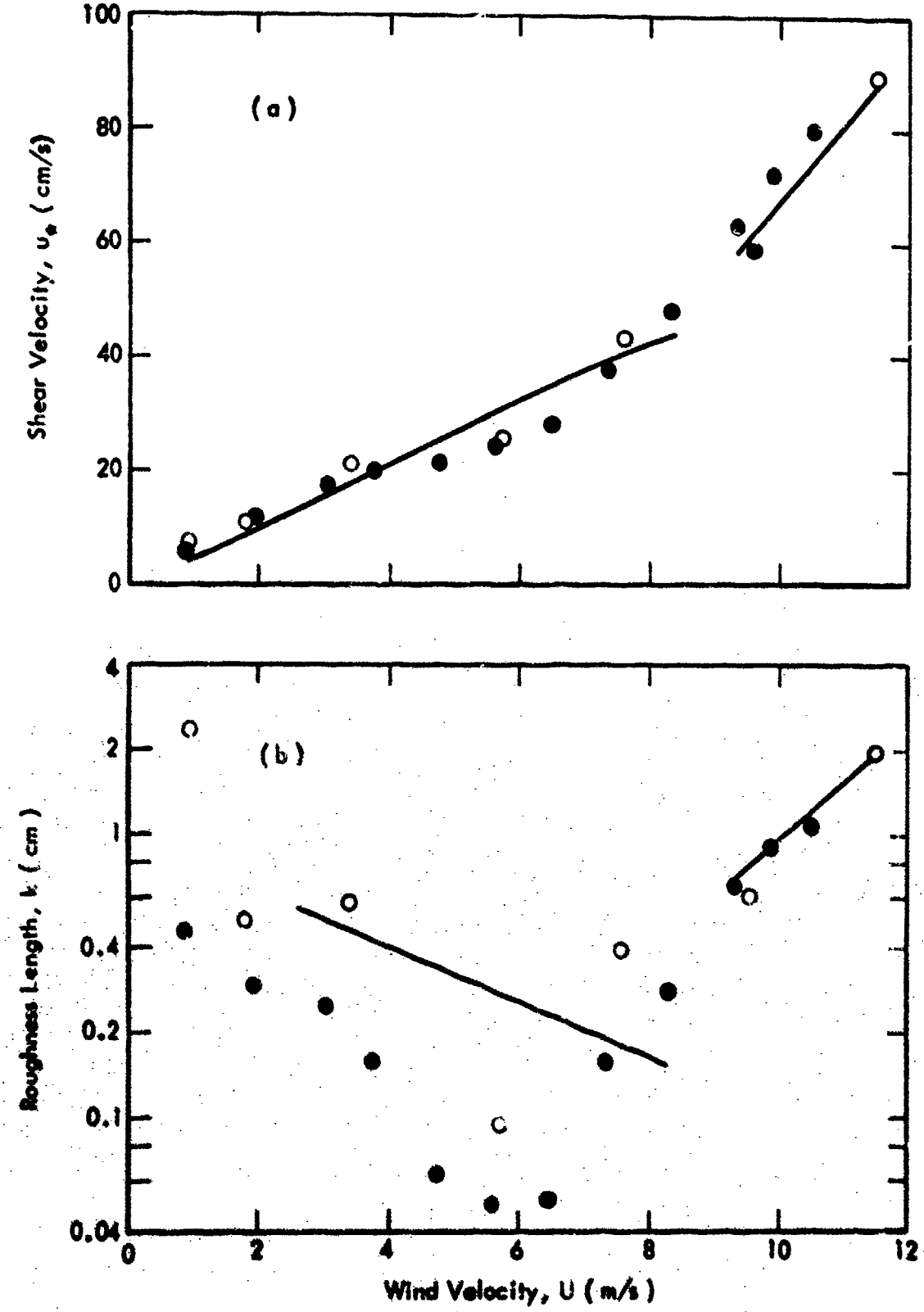

FIGURE 3 - SHEAR VELOCITIES AND ROUGHNESS LENGTH OF WIND OVER PRE-EXISTING WAVES OF LARGE AMPLITUDE (●) AND OF SMALL AMPLITUDES (o). The solid lines indicate the results obtained earlier (1973 b) without pre-existing waves.

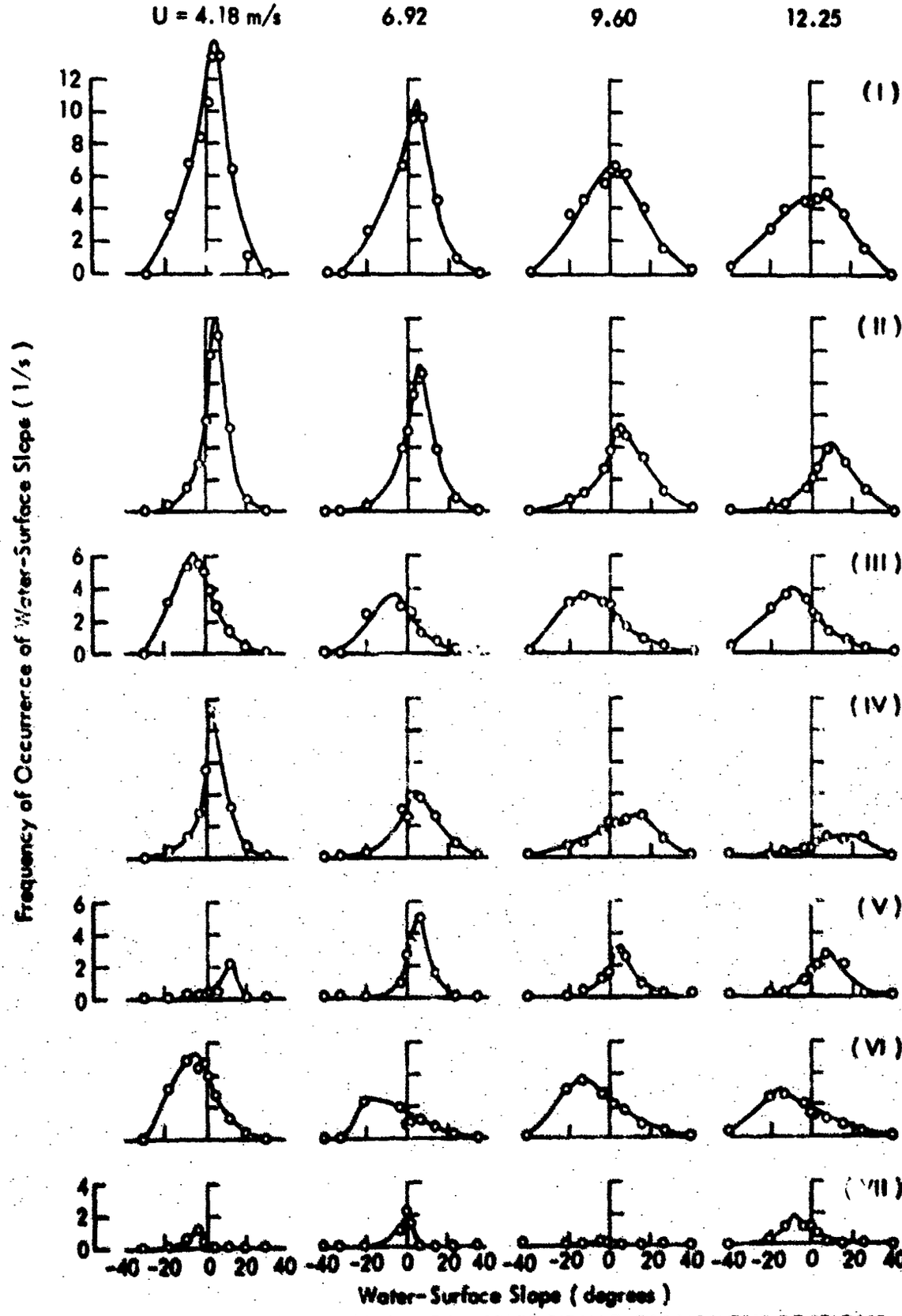

FIGURE 4 - SLOPE DISTRIBUTION OF RIPPLES RIDING ON VARIOUS PORTIONS OF CARRIER-WAVE PROFILES. The data were obtained from the following portions of the carrier-wave profile: (I) entire profile, (II) leeward face, (III) windward face, (IV) upper half of leeward face, (V) lower half of leeward face, (VI) upper half of windward face, (VII) lower half of windward face

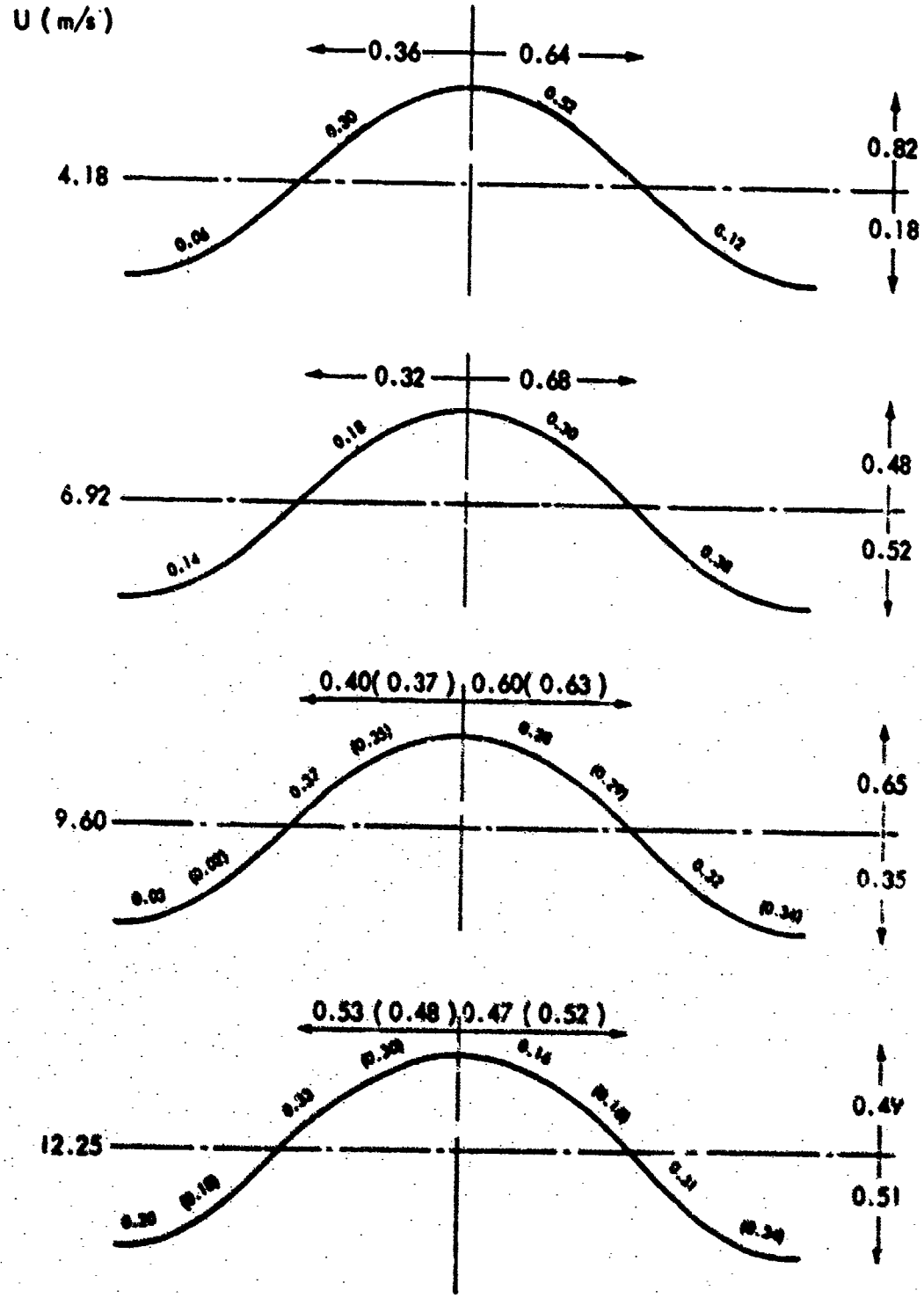

FIGURE 5 - DISTRIBUTIONS OF RIPPLES ALONG CARRIER-WAVE PROFILES. The wind direction is from left to right of the figure.

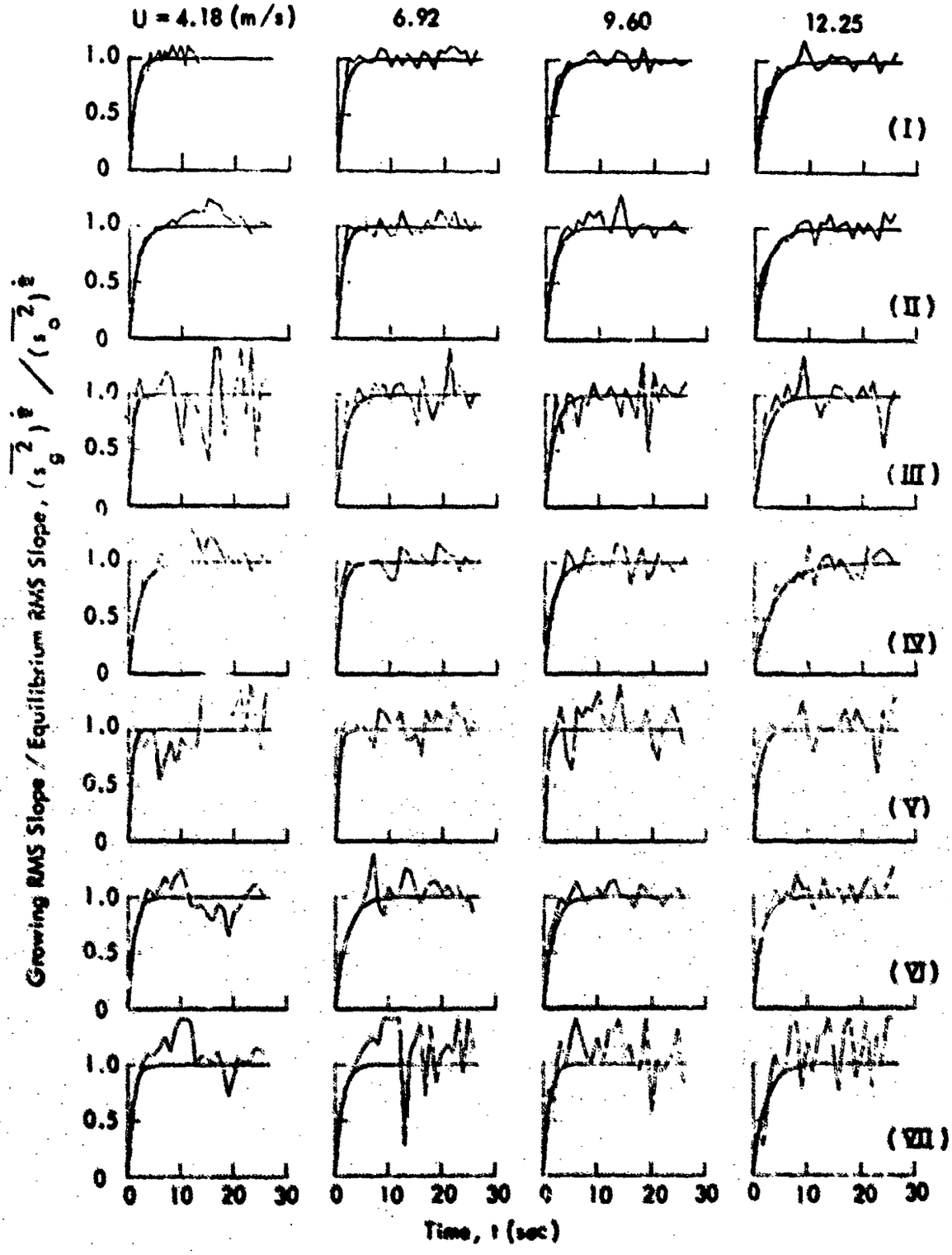

FIGURE 6 - EXPONENTIAL GROWTH OF ROOT-MEAN-SQUARE SLOPE FOLLOWING A SUDDEN WIND START. The row number shown on the right side of the figure is the same as that indicated in Figure 4.

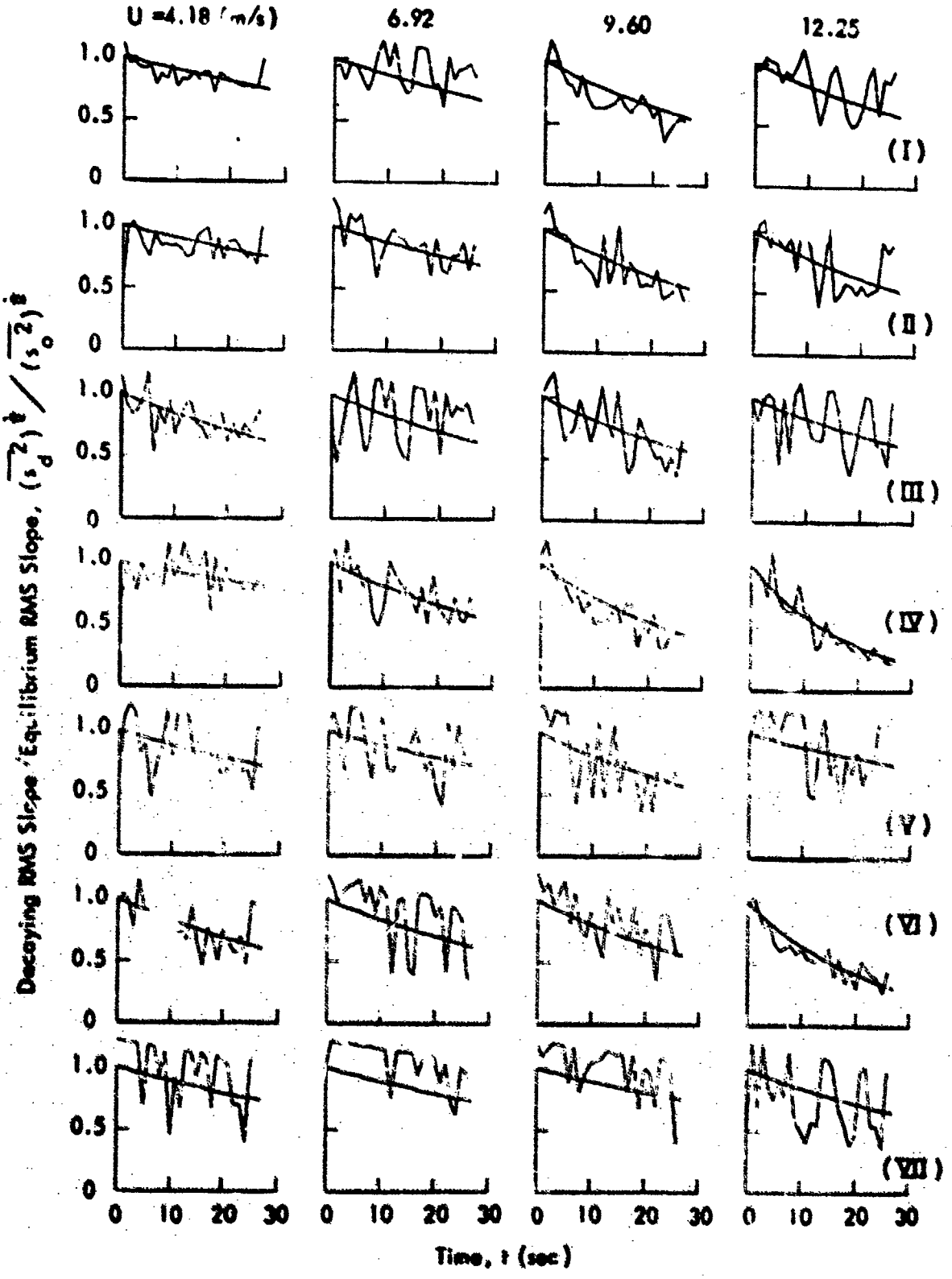

FIGURE 7 - EXPONENTIAL DECAY OF ROOT-MEAN-SQUARE SLOPE FOLLOWING A SUDDEN WIND STOPPAGE. The row number shown on the right side of the figure is the same as that indicated in Figure 4.

HYDRONAUTICS, Incorporated

DISTRIBUTION LIST
Contract No. N00014-72-C-0509
NR 062-472

Dr. J. D'Albora
Naval Underwater Systems Cen.
Newport, Rhode Island 02840 1

Johns Hopkins University
Applied Physics Laboratory
8621 Georgia Avenue
Silver Spring, Maryland 20910
Attn: L. Cronvich 1
H. Gilreath 1
A. Stone 1

University of California, SD
Marine Physical Laboratory
Scripps Inst. of Oceanography
San Diego, Calif. 92152
Attn: Dr. F. Spiess 1

Dr. Martin H. Bloom
Polytechnic Inst. of Brooklyn
Route 110
Farmingdale, N. Y. 11735 1

General Research Corporation
1501 Wilson Blvd., Suite 700
Arlington, Va. 22209
Attn: Mr. P. Donahoe 1

Dr. Marvin King
Riverside Research Inst.
80 West End Avenue
New York, New York 10023 1

Dr. James Young
Science Applications, Inc.
P.O. Box 2351
La Jolla, Calif. 92037 1

Mr. V. Lujetic
Tetra Tech, Inc.
1911 N. Ft Myer Drive
Arlington, Virginia 22209 1

University of California
Lawrence Livermore Laboratory
P. O. Box 808
Livermore, Calif. 94550
Attn: Dr. H. P. Smith 1
Dr. Michael Wirth 1

Dr. W. S. Lewellen
Aeronautical Res. Associates
of Princeton, Inc.
50 Washington Road
Princeton, New Jersey 08540 1

R&D Associates
P. O. Box 3580
Santa Monica, Calif. 90403
Attn: Dr. D. Holliday 1
Dr. F. L. Fernandez 1
Dr. M. Milder 1

Dr. K. V. Saunders
Pacific-Sierra Research Corp.
P. O. Box 578
Malibu, California 90625 1

Dr. Thomas Taylor
The Aerospace Corporation
P. O. Box 92957
Los Angeles, Calif. 90009 1

TRW Systems Group
One Space Park
Redondo Beach, Calif. 90278
Attn: J. Chang 1
E. Baum 1

Mr. L. W. Griswold
Naval Ship Research &
Development Center
Annapolis Laboratory
Annapolis, Md. 21402 1

Dr. Frank Lane
KLD Associates, Inc.
7 High Street, Suite 204
Huntington, New York 11743 1

Dr. M. Y. H. Pao
Flow Research, Inc.
1819 S. Central Ave., Suite 72
Kent, Washington 98031 1

Dr. D. R. S. Ko
Flow Research, Inc.
5959 West Century Blvd.
Los Angeles, Calif. 90045 1

HYDRONAUTICS, Incorporated
Pindell School Road
Howard County
Laurel, Maryland 20810
Attn: Dr. J. Wu 1
Dr. T. R. Sundaram 1

Xonics, Inc.
6837 Hayvenhurst Ave.
Van Nuys, California 91406
Attn: Dr. M. Balser 1

Dr. J. Alex Thomson
Physical Dynamics, Inc.
P. O. Box 1069
Berkeley, California 94701 1

Dr. Roberto Vaglio-Laurin
Advanced Technology Labs., Inc.
400 Jericho Turnpike
Jericho, New York 11753 1

Mr. R. Rehm
CALSPAN Corporation
P. O. Box 235
Buffalo, New York 14221 1

Stanford Research Institute
333 Ravenswood Avenue
Menlo Park, California 94025
Attn: H. Guthardt 1
K. Krishnan 1

Institute for Defense Analyses
400 Army Navy Drive
Arlington, Virginia 22202
Attn: Dr. P. A. Selwyn 1
Dr. Joel Bengston 1
Mr. J. C. Nolen 1

Naval Research Laboratory
4555 Overlook Avenue
Washington, D. C. 20390
Attn: F. MacDonald 1
J. O. Elliot 1
K. G. Williams 1
S. Piacsek 1
A. H. Schooley 1

Office of Naval Research
800 N. Quincy Street
Arlington, Virginia 22217
Attn: M. Cooper (438) 1
R. Cooper (438) 1
J. Witting (481) 1
Cdr. J. Ballou (466) 1
Dr. S. Reed (102T) 1

Naval Undersea Center
San Diego, California 92132
Attn: O. Lee 1
K. Nelson 1

Defense Advanced Research
Projects Agency
1400 Wilson Blvd.
Arlington, Virginia 22209
Attn: K. Kresa, TTO 1
S. Ruby, MATS 1
R. Hoglund, STO 1

ODDR&E
The Pentagon
Washington, D. C. 20301
Attn: D. R. Heebner, 3E1040 1
N. F. Wikner, 3E1087 1
G. Cann, 3D1048 1

Director
Central Intelligence Agency
Main Station
Washington, D. C. 20305
Attn: H. Farmer 1

Cdr. D. Walsh
OASN/R&D
The Pentagon, 4E471
Washington, D. C. 20350 1

Mr. D. A. Rogers
SP 2018/NSP
Department of the Navy
Washington, D. C. 20390 1

Cdr. R. Miller
Ofc Chief of Naval Operations
The Pentagon, 5D572
Washington, D. C. 20350 1

Captain D. Keech
Deputy Director of Navy Labs
Department of the Navy
Washington, D. C. 20360 1

Naval Scientific & Technical
Intelligence Center
4301 Suitland Road
Washington, D. C. 20390
Attn: Capt. J. P. Prisley 1

Mr. I. H. Gatzke
Naval Air Systems Command
Department of the Navy
Washington, D. C. 20360 1

Defense Documentation Center
Cameron Station
Alexandria, Virginia 22314 12